Michigan State University

National Superconducting Cyclotron Laboratory

TIME RESOLVED DIFFERENTIAL FRAGMENTATION CROSS SECTIONS OF C^{+}_{60} + C_{60} COLLISIONS

JÜRGEN SCHULTE

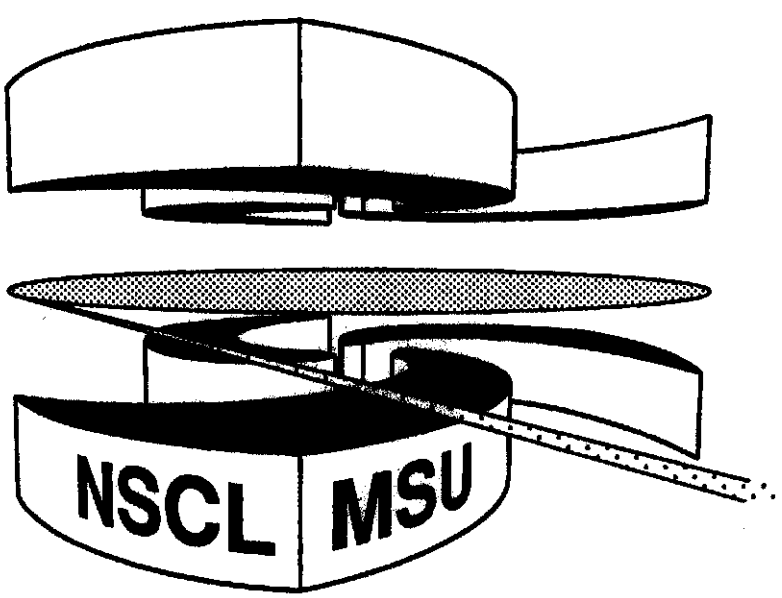

MSUCL-958

NOVEMBER 1994

Time Resolved Differential Fragmentation Cross Sections of C_{60}^{+} + C_{60} Collisions

Jürgen Schulte

National Superconducting Cyclotron Laboratory,

Michigan State University, East Lansing, MI 48824

E-mail:Schulte@rudolf.nscl.msu.edu

Abstract

The collision of thermally excited C_{60}^{+} with a cross beam gas target of C_{60} clusters has been simulated employing the Molecular Dynamics Statistical Trajectory Ensemble method and the DFT LCAO local density approximation. The time resolved double differential cross sections of the mass fragmentation and kinetic energy angular distribution, and the mass resolved fragment vibrational excitation and mean coordination number has been calculated with improved statistics from the newly available simulation data. The time resolved double differential cross sections show the causal order and other details of the fragmentation process. The fragmentation pattern of the small fragment sizes (N≤20) where this simulation has the most reliable statistics is given special attention.

PACS: 36.40+d, 35.10b,82.40d,32.80n

I. Introduction.

In a previous publication [1] we have presented first statistically acceptable results of a parameter free Molecular Dynamics Statistical Trajectory Ensemble (MDSTE) simulation of ${}^{*}C_{60}^{+} + C_{60}$ collisions (the * denotes that the clusters are thermally excited). The simulation resembles a cluster-cluster cross beam experiment similar to that performed by Campbell et al. [2]. In their experimental set up a beam of ${}^{*}C_{60}^{+}$ clusters, with an estimated 30 eV average thermal excitation energy, was crossed with a C_{60} gas target. The experiment was performed at some 10^2 *eV* center of mass (com) collision energy. The fragment mass distribution and the energy transfer of the resulting reaction products were measured. The experiment has shown good resolution of the fragment mass distribution for the larger fragments (N≥50), and low resolution for the small fragments (N≤20). In our simulation the situation is just reversed, i.e., we find acceptable resolution (statistics) for the smaller fragments, and still unacceptable statistics for medium size and very large fragments. The nature of this behavior is very obvious since our simulation provides a relatively small ${}^{*}C_{60}^{+}$ beam current (number of collision trajectories) only, however, the number of collision trajectories at our final simulation time step is sufficient large to provide a good resolution of the population of the small collision fragments. We have analyzed the thermal excitation, kinetic energy, internal structure (mean coordination number), and angular distribution as a function of fragment size and chronological course of the collision. The cross sections at the respective typical time steps were calculated from 1024 trajectories (t =0.098 *ps*), 192 trajectories (t=0.36 *ps*), 192 trajectories (t=1.08 *ps*), and 128 trajectories (t=2.1 *ps*), respectively.

Various investigations have been performed to study possible reaction paths of coagulating and colliding C_{60} molecules [3,4]. Only recently, however, the possibility of integrating over the entire reaction cross section of ensembles of colliding clusters and molecules, interacting via accurate many-body forces, has become available.

In this simulation for the electronic and ionic interaction of carbon atoms we have employed the DFT LCAO-LDA potential by Seifert and Jones [4], a hybrid of an empirical potential and the DFT LCAO-LDA approximation. This approach has been successfully applied to the simulation of ion-trap experiments on $C_2^+ + D_2$ [5], and to the deuterium capture in $C_{60} + D_2$ reactions [6], respectively.

The presented ${}^*C_{60}^+ + C_{60}$ collision simulation has been carried out at 500 eV com collision energy. Thus, the total kinetic energy per atom in this simulation is low enough (4.41 *eV*) such that electronic excitation is not expected to occur [1]. The DFT LCAO-LDA approximation of electronic interaction in this simulation is justified by the high collision energy where the energy per atom is in the *eV* range, i.e., there is no need for a full *ab initio* calculation to cover subtle *meV* details of the potential energy surface. The DFT LCAO-LDA potential accounts for the many-body characteristics important in the chemical bonded system that is encountering structures far from equilibrium where other parameterized potentials lack of reliability [1]. For a detailed discussion of the MDSTE simulation of cluster gas-phase and cluster-cross beam experiments see refs. [5] and [7], respectively.

A brief summary on the preparation of the clusters, and their respective collision trajectories, of the ${}^{*}C_{60}^{+} + C_{60}$ simulation is given in Section II. In Section III we present results of the MDSTE time resolved double differential fragmentation cross sections of the ${}^{*}C_{60}^{+} + C_{60}$ collision simulation at 500 *eV* center of mass collision energy. The chronological course of the fragmentation process is discussed by means of the double differential cross sections of the mass fragmentation and kinetic energy angular distribution, and the mass resolved fragment vibrational excitation and mean coordination number at a sequence of four typical simulation time steps (0.098 *ps*, 0.36 *ps*, 1.08 *ps*, 2.1 *ps*). At the last simulation time step (2.1 *ps*), when the main part of the fragmentation is believed to be finished [1], the fragmentation pattern of the smaller fragments (N≤20) is discussed in more detail. Our investigation on the fragmentation in ${}^{*}C_{60}^{+} + C_{60}$ collisions is summarized in Section IV.

II. Preparation of Trajectories.

The fragmentation cross section of the ${}^{*}C_{60}^{+} + C_{60}$ cross beam experiment is modeled by employing the Molecular Dynamics Statistical Trajectory Ensemble method developed for parallel computing [7]. For the interaction of carbon atoms we take the hybrid *ab initio* DFT LCAO-LDA potential [4]. In the DFT LCAO-LDA regime by Seifert and Jones [4] the bond energies are overestimated by factor of two. Thus, one has be careful with comparing absolute energies. There is no problem, however, with comparing energy differences such as represented in the bond breaking process and individual relative cluster stability.

The cross beam collision of the carbon clusters is modeled by an ensemble of collision trajectories where the initial conditions of every trajectory are taken from the proper statistical distribution. The initial geometric cluster configuration, for all C_{60} clusters, is the DFT LCAO-LDA fullerene equilibrium structure. The carbon atoms of every thermally excited cluster are given an internal Maxwell-Boltzmann velocity distribution such that the ensemble of thermally excited clusters has an initial mean internal cluster kinetic energy of 30 *eV*. The thermally excited clusters, and the cold clusters, are placed at a center of mass distance of 20 atomic units (*a.u.*), and were given 10 fixed impact parameters between 1 *a.u.* and 15 *a.u.* After an initial random rotation about the internal axes of the clusters, the clusters were given a relative collision velocity according the com collision energy of 500 *eV*. The equation of motion in the DFT LCAO-LDA scheme is calculated using the Verlet algorithm with a step size of Δt=50 *atu* (1 *atu* = 2.4×10^{-17} sec). Cross sections are calculated by integrating over all collision orientations, thermal excitations, and impact parameters.

From the statistical point of view, in order to achieve some meaningful fragmentation statistics, and convergence, one might expect to calculate a large number of trajectories for a system of 120 atoms. Fortunately, the studied system is not just composed of simple structureless 2-body interacting point particles, but of particles with electronic structure that favor strong directional chemical bonds. The simple combinatory assumption of fragmentation statistics obtains strong constraints by the geometry and the binding properties of the studied systems. Thus, the basic fragmentation characteristics can be shown with using a rather limited number (128-1024) of ensemble trajectories.

III. Double Differential Fragmentation Cross Sections of ${}^{*}C_{60}^{+} + C_{60}$ Collisions.

From the simulation data we were able to calculate double differential cross sections of the fragment mass and kinetic energy angular distribution, and the fragment mass resolved mean coordination number and vibrational excitation. Fig 1-4 show the time resolved double differential cross sections of the ${}^{*}C_{60}^{+} + C_{60}$ collision reactions at four typical time steps (0.098 *ps*, 0.36 *ps*, 1.08 *ps*, 2.1 *ps*) of the collision. Fig. 5 shows the time resolved fragmentation cross section (mass spectrum) at the corresponding time steps. In the following with respect to kinetic energies (translational and vibrational), we are always referring to the respective mean kinetic energy per atom. In this context with quasi-elastic, inelastic and deep inelastic collision, we are referring to ${}^{*}C_{60}^{+} + C_{60}$ collisions that have suffered energy loss to vibrational excitation of fully intact C_{60} clusters, to collisions where one or both of the colliding C_{60} clusters have lost a minor amount (≤ 4) of atoms only, and to collisions where one or both of the colliding clusters have suffered severe fragmentation or loss of the original structure.

At the very beginning of the collision (0.098 *ps*, Fig. 1) where some of the colliding C_{60} clusters are starting to encounter quasi-elastic and deep inelastic collisions we observe an almost uniform angular distribution of the immediate release of carbon monomers and dimers (Fig. 1a). The translational kinetic energy of the dimers is scattered within a range

of up to 9 *eV* with a little cross section enhancement around the mean of the dimer kinetic energy of E_k=2.4 *eV* (Fig. 1c). Notice that the initially available total mean kinetic energy per atom is 4.41 *eV*, i.e., around 2.2 eV in each of the C_{60} clusters. Independent from the dimers' kinetic energy all the dimers have been released thermally extremely cold (Fig. 1b), i.e., with a vibrational energy of 1/10 ($\leq$ 0.05 *eV*) of the initially available vibrational energy stored in the ionized $^{*}C_{60}^{+}$ cluster. The corresponding parent clusters (N=58, N=118) are found with mean thermal excitation energies of E^{*}=2.1 *eV*, suggesting that the dimers may have been released in a sputtering process or an uncompleted thermalization process. In all of our considerations on the kinetic excitation energy we are neglecting the small amount of rotational energy contained in E^{*} [8]. Prior to their release some of the produced dimers may have been involved in pre-collision 2+2 cycloaddition and 2+4 cycloaddition processes as suggested by Strout et al. [9], i.e., C_2 bridging between the C_{60} molecules, and subsequently being pushed out of the collision area, probably with translational kinetic energies according the local temperature.

It is interesting to see that at this point of the simulation both the quasi-elastic scattered C_{60} and the deep inelastic collision encountering large $C_{\geq 116}$ compounds have a mean vibrational excitation of E^{*}=2.1 *eV* (Fig. 1b). In the quasi-elastic scattered clusters and the large compounds approximately 50% of the available translational kinetic energy has been transferred into vibrational modes.

From the mass resolved mean coordination number cross sections n_c conclusions on the geometric structure and geometric distortion of the C_{60}'s and their fragments, respectively, can be drawn. Fig. 1d shows that at this time step of the ensemble collision simulation the quasi-elastic scattered C_{60} and the deep inelastic collisions encountering large $C_{N\geq 116}$

compounds have maintained the fullerene-like 3-coordinated geometrical structure. Only few deviations from the 3-coordinated structure can be observed indicating that some fullerene structures have just been opened, or a have not been closed again yet. The close correlation of the cross sections shown in Fig. 1b and Fig. 1d, respectively, indicates that there is a strong coupling of the vibrational excitation of the clusters, and fragments, and their corresponding geometric structures.

With the collision proceeding, under the load of the collision moment the large cluster compounds lose their structural integrity as well as fragment into smaller clusters. As a consequence the cross sections of the small fragment ($N \leq 10$) sizes and the corresponding remainder cluster sizes ($48 \leq N \leq 64$, $N \geq 110$, Fig. 5, $t=0.36\ ps$) are starting to populate. Due to the finite maximum impact parameter in our simulation we find the quasi-elastic and inelastic scattered parent clusters of size $N \approx 60$ at com scattering angles of around $\theta=20$ and $\theta=160$ (Fig. 2a), respectively. Though at this point of the simulation where the clusters are still heavily involved in deep inelastic collision and fragmentation, and a general statement on the angular scattering of small fragments cannot be made yet, we like to point out the starting cross section enhancement of dimer scattering into the $\theta \approx 80$ region. Following the course of the time sequences of this simulation we shall see that it is possible to link the dimer fragments to the enhanced $\theta \approx 80$ scattering that has been found in a low statistics evaluation of the first 32 available trajectories of this simulation [10]. With the improved resolution and statistics of the MDSTE simulation presented here, we shall see that the $\theta \approx 80$ scattering found in [10] can no longer be linked to a general collective flow of carbon matter as stated in [10].

The very small cluster fragments (N≤4) are found thermally rather cold ($E^* \leq 0.5eV$, Fig. 2b), and therefore very unlikely to experience further fragmentation. Fig. 2b shows that the mean vibrational excitation E^* of the large cluster compounds has lost approximately 1 *eV* over the past 0.32 *ps* of our simulation. Some of the excitation energy has been lost due to the emission of small fragments, however, most excitation energy has been lost to the geometrical restructuring procedure resulting in a general decrease of the corresponding n_c cross sections (Fig. 2d). We find the large cluster compounds loosing their structural integrity by opening the fullerene cage and forming $n_c \approx 2.5$ objects as indicated by the cross section island (Fig. 2d) at N≥110. These more open structures are fullerene-like structures and intertwined carbon chains similar to those found near T_c in the thermal bath simulation of evaporating isolated C_{60} clusters by Gon and Tománek [11]. In the deep inelastic collisions that resulted in large cluster compounds almost all collisional kinetic energy has been transformed ($E_k \leq 0.1$ eV, Fig. 2c) into potential energy used for the restructuring processes.

Notice that in Figs. 2-4 the scales of the cross section axis differ from the scales shown in Fig. 1. We have adjusted the scales for better visualization of individual cross sections.

The quasi-elastic and inelastic scattering of the fullerenes appears to be completed at the simulation time step t=1.08*ps*, i.e., we observe no further increase of the cross sections at their respective scattering angles (θ=20, θ=160, Fig 3a). The dimer release into the $\theta \approx 80$ region has manifested itself very clearly, where there is only little contribution by other fragment sizes to this scattering region. Notice that 50% of the $\theta \approx 80$ angular scattering

cross section at this time step had been contributed by the former very early (t=0.36 *ps*), released dimers.

The close correlation of the vibrational excitation cross section (Fig. 3b) and the geometric structure, as represented in the n_c cross section (Fig. 3d), has been fairly maintained during the whole course of the collision history. Thus, we may conclude that the fragments suffered no, or only little, secondary collision or coagulation so far. Fig. 3b shows that the collision fragments are vibrationally excited with mainly two (1 *eV* and 1.5 *eV*) distinct average vibrational excitation energies. The quasi-elastic and inelastic scattered fullerenes populate the cross section of the E^*=1.5 *eV* excitation. The small and medium size fragments, and the large compounds are excited E^*=1 *eV* . Thus, we conclude that the medium and small size fragments formed at this time step are fragmentation products of the large slow moving ($E_k \leq 0.1$ *eV*) cluster compounds that, as a remainder of the former parent compounds, used to be in thermal equilibrium with their prospected fragments (E^*=1 *eV*). From Fig. 3d we see that basically only two distinct geometrical structures (characterized by their n_c-value) have been formed, fullerene-like and intertwined carbon chain structures (n_c>2.5), and elongated pure chain-like structures ($n_c \approx 2$), respectively. Unlike assumed in a previous publication [1], the large compounds do not contribute to the population of the cross section of the fullerene-like structures. Also, having a mean coordination number $n_c \approx 2$ the large compounds seem to have relaxed to rather long carbon chains than to open fullerene-like or intertwined carbon chain objects.

The distribution of the translational kinetic energy cross sections of the small and medium size fragments (Fig. 3b) seems to follow a line of the energy distribution of an ideal cluster gas, however, the fragments have to undergo some few more collisions in order to

resemble the ideal cluster gas situation. Notice that the most frequent small cluster fragments (Figs. 3c and 5; even numbered cluster sizes) show considerable large cross sections for kinetic energies around 1 *eV* confirming the ongoing thermalization fragmentation process in the large cluster compounds stated above.

Comparing the mean coordination number cross sections n_c in Figs. 3d and 4d, and the corresponding fragmentation cross sections in Fig. 5, one can see that most of the spectacular part of the fragmentation process in our ensemble collision simulation has been finished at t=2.1*ps*. The cross sections of the small clusters have stabilized, and an odd-even alteration in the fragmentation mass spectrum is clearly visible (Fig. 5, t=2.1*ps*). The relatively low vibrational excitation of the small and medium size fragments does not suggest that subsequent collision processes have occurred.

Fig. 4b shows the quasi-elastic and inelastic scattered N≈60 with E^*=2.1 *eV* vibrational energy have lost considerable ($\Delta\sigma$=210 $(a.u.)^2$) cross section compared to the cross section at time step t=1.08 *ps* (Fig. 3b). These clusters have suffered multifragmentation processes resulting in the population of the cross section of small and medium size fragments. During this delayed multifragmentation process also N=10 fragments have been formed which were not populated very much at t=1.08 *ps* (Fig. 5, σ<5 $(a.u.)^2$). Now we find N=10 fragments with more than tripled cross section forming a distinct cross section peak compared to the neighboring cross sections of even numbered fragments (Fig. 5, σ<16 $(a.u.)^2$). It is likely that some of the larger compounds have contributed to the increase of the N=10 cross section too, however, due to the very low total cross section of larger

compounds their contribution to the N=10 cross section is of minor importance and therefore leaves only the N≈60 clusters as the main source of this fragmentation channel.

In Fig. 4b, besides the quasi-elastic and inelastic collisions with the E^*=2.1 *eV* vibrational excitation, we find the cross sections of the vibrational excitation energy of the fragments show two additional regions of preferred excitation energies for small and medium (N<50) size fragments. In one region the vibrational energy follows a f(c/N) functional dependence that converges to a E^*=1 *eV* vibrational excitation, in the other region the vibrational excitation is E^*=1 *eV* independent of the size of the cluster fragments.

Looking at the total differential translational energy cross section (Fig. 6a) we see that besides the quasi-elastic and inelastic cross section peak at E_k=2.2 *eV* we find a distinct enhancement of cross section at E_k=1 *eV* (Fig. 6, t=2.1*ps*) with a clear separation (see arrow in Fig. 6) to the E_k=2.2 *eV* cross section peak. Since only very few large compounds were left at the previous time step (Fig. 5, t=1.08*ps*), we conclude that most of the contribution to the increase of the small fragment cross sections is due to fragments originated in fully intact (Fig. 3d) quasi-elastic scattered C_{60} clusters with E^*=2.1 *eV* vibrationally and E_k=2.2 *eV* translational kinetic energy (Figs. 3c and 4c), respectively. During this last simulation step excitation energy accumulated during the quasi-elastic collisions has been used for structural reorganization (open fullerene-like, intertwined carbon chain) and bond-breaking (fragmentation) processes resulting in an almost thermalized cluster gas with mean E_k≈1 *eV*.

From the double differential cross sections of this last simulation time step, where the collision and fragmentation process may be considered to be finished [1], we conclude that a large fraction of the cluster fragments have been formed during a starting isothermal-like cluster gas expansion following the quasi-elastic and inelastic collisions. The fragmentation products of this process show a kinetic energy distribution with the vibrationally highly excited quasi-elastic and inelastic scattered clusters as thermal source. Some of the dimer fragments may have been formed in a sputtering-like process during the onset of the collision. Small and medium size fragments have also been formed during a thermalization process of vibrational excited large cluster compounds, and give rise to an additional kinetic energy distribution with the vibrational excited large cluster compounds as another thermal source. The two processes can be resolved only at the end of the primary collision process where the statistics of the two fragmentation processes can be separated due to the larger population of the onset of an isothermal cluster gas expansion. Since in the MDSTE simulation we follow ${}^{*}C_{60}^{+} + C_{60}$ trajectories up to a simulation time step t=2.1 *ps*, and do not follow individual subsequent fragment trajectories colliding with other sets of ${}^{*}C_{60}^{+} + C_{60}$ collision trajectories, in our simulation we observe only the very first step of a cluster gas formation. Thus, due to missing secondary, and subsequent, collisions the kinetic energy distributions are not completely equilibrated yet. The many-body interaction and the carbon chemical bonds, however, introduce sufficient constraints that cause a rapid adjustment of vibrational energy and translational kinetic energy. This behavior makes it possible to obtain meaningful statistics even with a very limit number of collisions (n_{tr}=128) and fragmentation (n_f=577) events at this time step.

At this final time step of our simulation it is worthwhile to note that the angular scattering of dimers into the θ=80 region (Fig. 4a) has not changed very much compared to the previous time step. Also, there is only a negligible contribution to the θ=80 angular cross section by other fragments. Considering that the value of the total dimer cross section is by a factor of 2 larger than the combined total fragmentation cross sections of the $2<N\leq10$ fragments, and considering the directional scattering nature of the dimers, we conclude that the collective carbon matter flow found in [10] is mostly due to directional dimer scattering, and may not necessarily be linked to a general directional flow of fragmenting carbon matter. Also, looking at the mean translational kinetic energy per atom E_k of the small fragments $N\leq28$ (Fig. 6b), we find that the com E_k distribution follows closely the kinetic com energy distribution with the E^*=2.1 *eV* vibrationally excited C_{60} clusters as the thermal source. Only for the prominent populated cluster fragments in the medium size range $10\leq N\leq20$ we find some deviation from the ideal thermal cluster gas distribution. One has to consider, however, that these frequently produced cluster fragments have not had any secondary, or subsequent, collisions yet. Thus, from the overall picture of the kinetic energy distribution we cannot confirm the presents of an additional thermal source such as a general collective flow of carbon matter present in the ${}^{*}C_{60}^{+} + C_{60}$ collisions as stated by Schmidt et al. [10].

In a recent experiment by LeBrun et al. [12] on the multifragmentation of C_{60} clusters a power-law fall-off in the production cross section of small carbon fragments, $\sigma(C_N) \propto N^{-\lambda}$, has been discussed for fragment sizes $N\leq20$. In this experiment a vapor target of C_{60} clusters has been bombarded with highly ionized Xe ions with center of mass

energies of some hundred MeV. In both the experiment and the accompanying fragmentation model based on a two-dimensional bond-percolation calculation a scaling coefficient $\lambda \approx 1.3$ has been found. LeBrun et al. compared the scaling coefficient found in the C_{60} fragmentation process to the critical exponent $\tau = 2$ known from percolation and phase transition theory, and to the critical exponent $\lambda \approx 2.6$ found in nuclear fragmentation experiments [13]. In our *ab initio* based simulation with a fit along the envelop of the most prominent fragmentation cross sections at the final time-step (Fig. 5, 2.1 *ps*) we find $\lambda \approx 1.47$ for fragment sizes N≤20. It is interesting to see that the value of λ is significant lower than τ for both the simple bond-percolation model calculation and the presented elaborated simulation. In the bond-percolation model calculation the authors attributed the low λ-value to the finiteness and the periodic boundary conditions of the model fullerene. Since we are studying the same system our simulation is based on the same constraints. We prefer, however, to speak of C_{60} clusters as topological two-dimensional objects instead of objects with periodic boundaries. The C_{60} clusters are consisting of almost surface only, thus we may as well consider the fragmentation process as a "surface ablation" process. In fact in our model simulation we may speak of an one-step ablation process considering the C_{60} clusters do not have a filled core, and very few secondary fragment collisions have been observed in our simulation.

Notice that our fragmentation scaling coefficient is close to the scaling coefficient $\lambda = 1.68$ found in high energy collision of basalt on basalt [14], and as well close to the scaling coefficient $\lambda = 1.70$ found in data of the mass distribution of asteroids in the planetary system [15]. Considering the fragmentation of asteroids and basalt as a combination of a weathering and ablation process Hüfner and Mukhopadhya [16] have shown that for these

fragmentation processes the value of the scaling coefficient λ is always smaller than two. Hüfner and Mukhopadhya assumed that the colliding basalt stones crash into a fragmentation distribution $D(m,\Delta)$ with m being the fragment mass, Δ the step-number of subsequent collisions, and $D(m,0)=\delta(m-M)$. During the crashing process a fraction q of the distribution, presumably the surface, is ablated and the remainder $(1-q)D(m,\Delta)$ is again crushed into $(1-q)D(m,2\Delta)$, and the fraction $q(1-q)D(m,\Delta)$ is in turn ablated and so forth. The resulting fragmentation distribution is the sum of all ablated matter [16],

$$D(m)=q\sum_{n=1}^{\infty}(1-q)^{n-1}D(m,n\Delta). \tag{1}$$

Assuming that the fragmentation distribution $D(m,\Delta)$ in eq. (1) follows the Kolmogorov scaling theory and weathering distribution [17],

$$D(m,n\Delta)=\frac{3-a}{M(n-1)!}\left(\frac{M}{m}\right)^{a-1}\times\left[(3-a)\ln\left(\frac{M}{m}\right)\right]^{n-1}\theta(M-m), \tag{2}$$

Hüfner and Mukhopadhya found that eq. (1) results in

$$D(m)=\frac{3-a}{M}q\left(\frac{M}{m}\right)^{2-q(3-a)}, \tag{3}$$

which is a pure power-law distribution, i.e., no logarithmic terms are involved. Notice that only for a one-step weathering process , i.e., no subsequent weathering and crushing, eq. (2) will result in a power-law $m^{-\lambda}$ as well, with $\lambda=a-1$. In fact, if we

assume that in the Hüfner and Mukhopadhya weathering-ablation process (eq.(3)) almost all matter follows the ablation fragmentation path, i.e., $q \to 1$, eq. (3) approaches the one-step process power law of eq. (2). The parameter a depends on the fragmentation physics, and mass conservation requires it to be less than three which means $\lambda < 2$. If in our simulation we would have found subsequent collision induced fragmentation, or if there were an additional source of collision available (such as molecules inside the C_{60} cage, or C_N molecules from other C_{60} fragmentation processes on collision trajectories), i.e., $q < 1$, we would have found a λ-value larger than $\lambda \approx 1.47$. If in our simulation we assume the one-step fragmentation parameter a found in our simulation ($a = 2.47$) being characteristic for the fragmentation of small carbon clusters, and if we further assume that (compact as well as fullerene-like) carbon clusters follow in general a fragmentation process according eq. (3), a hypothetical ablation ratio of $q = 0.56$ would result in same power-law exponent $\lambda \approx 1.7$ as has been found for basalt and asteroids, respectively. In such an assumed collision of carbon matter, an average 40% of each collision remainder would serve as new large core of subsequent collisions.

If we assume a pure weathering fragmentation process according to eq. (2), due to the very finite size of the molecular clusters considered, only a limited number $n\Delta$ of subsequent collision-fragmentation processes are available, and correspondingly few overlapping distributions will contribute to the total fragmentation spectrum. Thus, the power law receives some logarithmic corrections, however, it would still be the leading term.

It would be interesting to see at what size carbon clusters show a characteristic fragmentation (bulk) coefficient and whether it converges to $\lambda \approx 1.7$. As well interesting

would be to see from what size on, at sufficient high collision energy, carbon clusters follow the percolation and phase transition theory, i.e., $\lambda \geq 2$.

IV. Summary.

We have investigated the fragmentation of C_{60} clusters in a ${}^{*}C_{60}^{+} + C_{60}$ cross beam experiment at 500 *eV* com collision energy. The presented simulation shows that collision momentum is transferred to internal vibrational energy immediately when the clusters start to encounter quasi-elastic and inelastic collisions (t=0.039 *ps*). At the moment of collision contact local overheating causes sputtering, or even explosive boiling processes [18], resulting in the release of a large amount of cold carbon dimers with high kinetic energy and a preferable com scattering angle (θ≈80). With the inelastic collisions proceeding large cluster compounds form (t=0.36 *ps*) and some fullerenes lose their structural integrity causing the formation of fullerene-like objects and intertwined carbon chains (n_c≈2.5). This restructuring process has taken internal kinetic energy from the large compounds, and is part of an beginning equilibration process. During this process small size fragments (N≤10) with preferable high translational energy (E_k≥2 eV) are released. The monitoring of the mean coordination number cross section nc has been proved very useful in this simulation.

With the inelastic and deep inelastic collisions proceeding the trend of the fragmentation process can be observed at a remarkably early state (t=0.36 *ps*) of the collision process. The thermally very excited C_{60} clusters and the large compounds undergo further

structural metamorphosis towards long intertwined carbon chains. This process takes time and internal kinetic energy, and very soon we find the fragments having almost fixed internal energies of E^*=1 *eV* over a wide range of fragment sizes ($10 \leq N \leq 104$). The internal energies of some small fragments ($N<10$) differ in the sense that they show an increase of thermal energy with increasing cluster size converging to a thermal energy of E^*=1 *eV*. We find two different distributions of internal energies which suggests the presence of two principle fragmentation processes. One fragmentation process that is part of an ongoing fragment internal equilibration process of large cluster compounds, and one that is part of an equilibration and delayed decay processes of thermally highly excited quasi-elastic and inelastic scattered $^{126eV}C_{60}$ clusters. The kinetic energy distribution of the fragments, together with a directional scattering for dimers only, does not suggest the presence of a collective flow in the $^{*}C_{60}^{+} + C_{60}$ collision fragmentation.

A fit along the envelope of the prominent small fragment sizes $N \leq 20$ shows the scaling behavior $\sigma(C_N) \propto N^{-\lambda}$ with λ=1.47. The scaling behavior has been discussed in terms of weathering and ablation fragmentation processes, and we have speculated that with more compact and larger carbon clusters the scaling coefficient may approach the one ($\lambda \approx 1.7$) found for bulk objects like basalt stones or asteroids. Further investigation is required to determine how large the collision energy and the colliding clusters have to be in order show a liquid-gas phase transition scaling with $\lambda \approx \tau \geq 2$.

Finally, this simulation has shown that the MDSTE approach along with appropriate interaction potentials is a useful tool shed more insight into general questions of collision and fragmentation processes.

Acknowledgment.

Part of this work has been supported by NATO, grant No. CRG 930351. The author is grateful to the Computer Science Departments at Texas A&M University and Michigan State University, the Parallel Computing Divisions of the San Diego Supercomputer Center, and the Computer Science Division at the Sandia National Laboratory for providing computational grants on their local parallel computers. The author is also grateful to G. Seifert for providing the basic frame of the originally sequential LCAO-LDA code.

Figure Capture.

Fig. 1: Double differential fragmentation cross sections σ (in $(a.u.)^2$)of the simulated ${}^{*}C_{60}^{+} + C_{60}$ collisions at simulation time step $t = 0.038\ ps$; (a) mass resolved center of mass angular scattering (θ), (b) mass resolved vibrational excitation energy per atom (E^{*}/eV), (c) mass resolved translational kinetic energy per atom (E_k/eV), (d) mass resolved mean coordination number (n_c).

Fig. 2: Double differential fragmentation cross sections of the simulated ${}^{*}C_{60}^{+} + C_{60}$ collisions at simulation time step $t = 0.36\ ps$; (a)-(d) as in Figure 1.

Fig. 3: Double differential fragmentation cross sections of the simulated ${}^{*}C_{60}^{+} + C_{60}$ collisions at simulation time step $t = 1.08\ ps$; (a)-(d) as in Figure 1.

Fig. 4: Double differential fragmentation cross sections of the simulated ${}^{*}C_{60}^{+} + C_{60}$ collisions at simulation time step $t = 2.1\ ps$; (a)-(d) as in Figure 1.

Fig. 5: Differential fragmentation cross sections (in $(a.u.)^2$) of the simulated ${}^{*}C_{60}^{+} + C_{60}$ collisions at simulation time step $t = 0.039\ ps$, $t = 0.36\ ps$, $t = 0.78\ ps$, $t = 1.08\ ps$, and $t = 2.1\ ps$, respectively.

Fig. 6: (a) Differential com translational kinetic energy cross section (in $(a.u.)^2$) of the simulated ${}^{*}C_{60}^{+} + C_{60}$ collisions at simulation time steps $t = 0.36\ ps$, $t = 1.08\ ps$ and $= 2.1\ ps$, respectively. (b) Mean translational kinetic energy distribution of the small and medium size fragments at $t = 2.1\ ps$. The solid line represents corresponding values assuming the large amount of vibrational excited ${}^{126eV}C_{60}$ clusters as thermal source.

[1] J. Schulte, Phys. Rev. **B**, Nov. 1994.

[2] E.E.B. Campbell, V. Schyja, R. Ehlich, I.V. Hertel,
Phys. Rev. Lett. **70**, 263 (1993).

[3] D.L. Strout, R.L. Murry, C. Wu, W.C. Eckhoff, G.K. Odom, G.E. Scuseria,
Chem. Phys. Lett. **214** (6), 576 (1993).
P. Ballone, P. Milani, Z. Phys. **D19**, 439 (1991).

[4] G. Seifert, R. O. Jones, Z. Phys. **D20**, 77 (1991).

[5] J. Schulte, G.Seifert, Chem. Phys. Lett. **221**, 230 (1994).

[6] G. Seifert, J. Schulte, Phys. Lett. **A188**, 365 (1994).

[7] J. Schulte, J. Appl. Physics, **75** (11), 7195 (1994).

[8] R. Ehlich, E.E.B. Campbell, O. Knospe, R. Schmidt, Z. Phys. **D28**, 153 (1993).

[9] D.L. Strout, R.L. Murry, C.Xu, W.C. Eckhoff, G.K. Odom, G. E. Scuseria,
Chem. Phys. Lett. **214**(6), 576 (1993).

[10] R.Schmidt, J. Schulte, G.Seifert, O.Knospe, Phys. Lett. A, in print.
J. Schulte, O. Knospe, G. Seifert, R. Schmidt, Phys. Lett. A, in print.

[11] S.G. Gon, D. Tománek, Phys. Rev. Lett. 72(15), 2418 (1994).

[12] T. LeBrun, H.G. Berry, R.W. Dunford, H. Esbensen, D.S. Gemmell, E.P. Kanter,
W. Bauer, Phys. Rev. Lett. **72**, 3965 (1994).

[13] A. Hirsch et al., Phys. Rev. **C29**, 508 (1984),
L.Phair, W. Bauer, C.K. Gelbke, Phys. Rev. Lett. **B314**, 271 (1993).

[14] H.J. Moore. D.E. GAult, Ann. Prog. Rep. (Astrogeological Studies),
US Geolog. Survey, Part B, p. 127 (1965).

[15] J.S. Dohnanyi, J. Geophys. Res. **74**, 2531 (1969),

J.S. Dohnanyi, J. Geophys. Res. **75**, 3468 (1970).

[16] J. Hüfner, D. Mukhopadhyay, Phys. Lett. **B173** (4), 373 (1986).

[17] A.N. Kolmogorov, C.R. Dokl. Akad. Nauk. SSSR XXXI, 99 (1949).

[18] H.M. Urbrassek, Nuclear Instr. and Methods in Physics Research **B31**, 541 (1988).

C.T. Avendisian. J. Chem. Ref. Data **14**, 695 (1985).

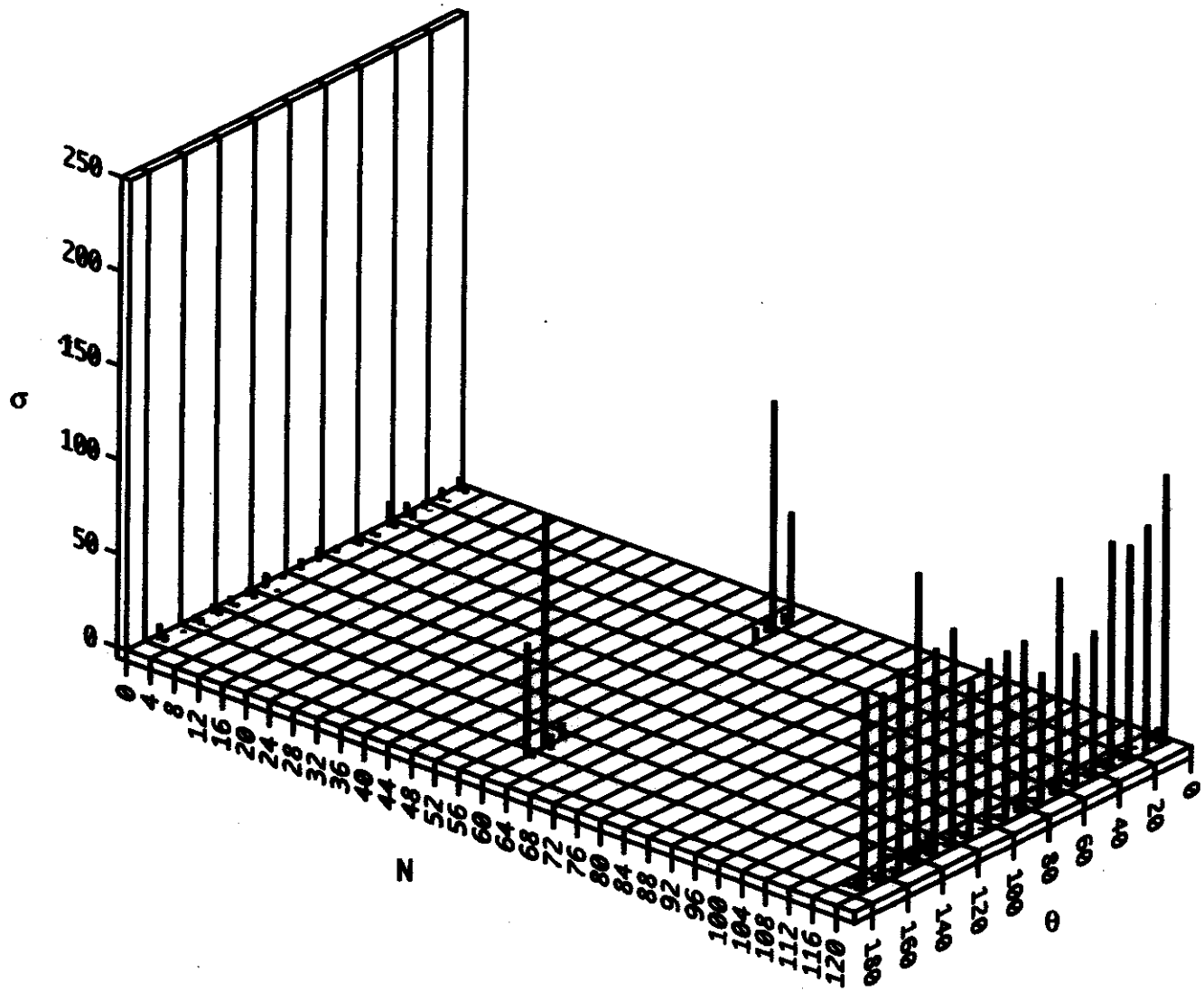

J. Schulte, Phys. Rev. B, Fig. 1a

(0.039 ps)

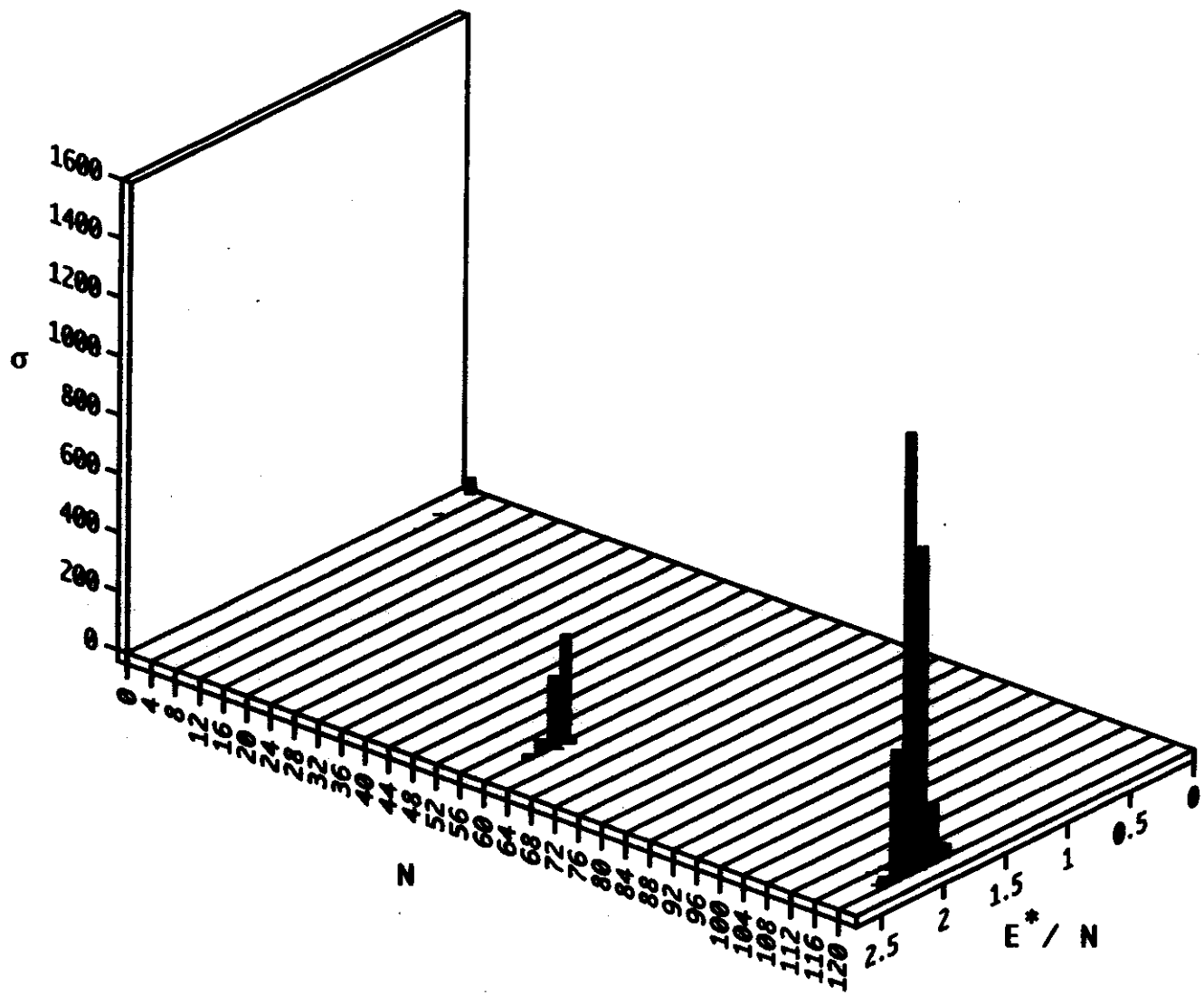

J. Schulte, Phys. Rev. B, Fig. 1b

(0.039 ps)

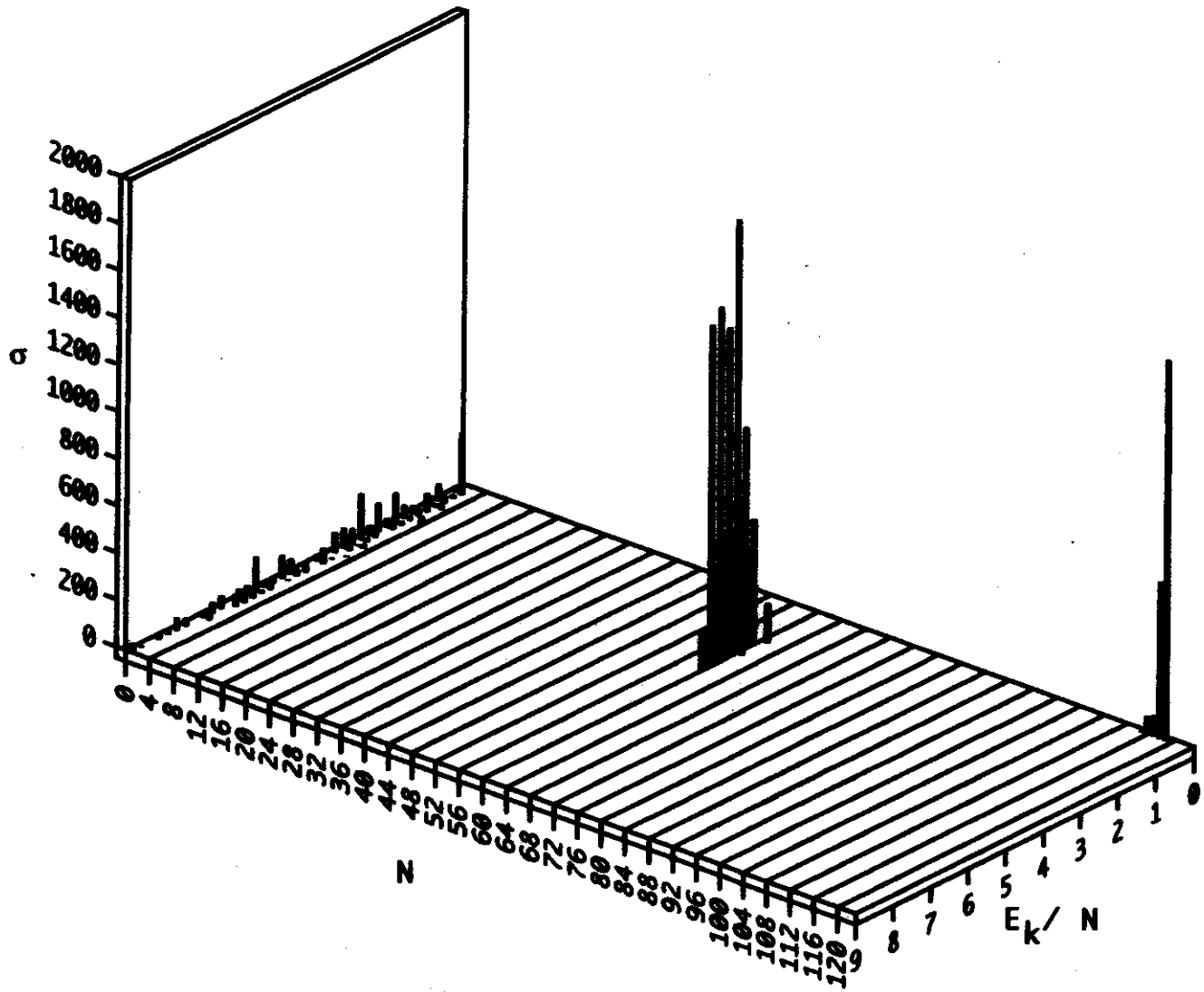

J. Schulte, Phys. Rev. B, Fig. 1c

(0.039 ps)

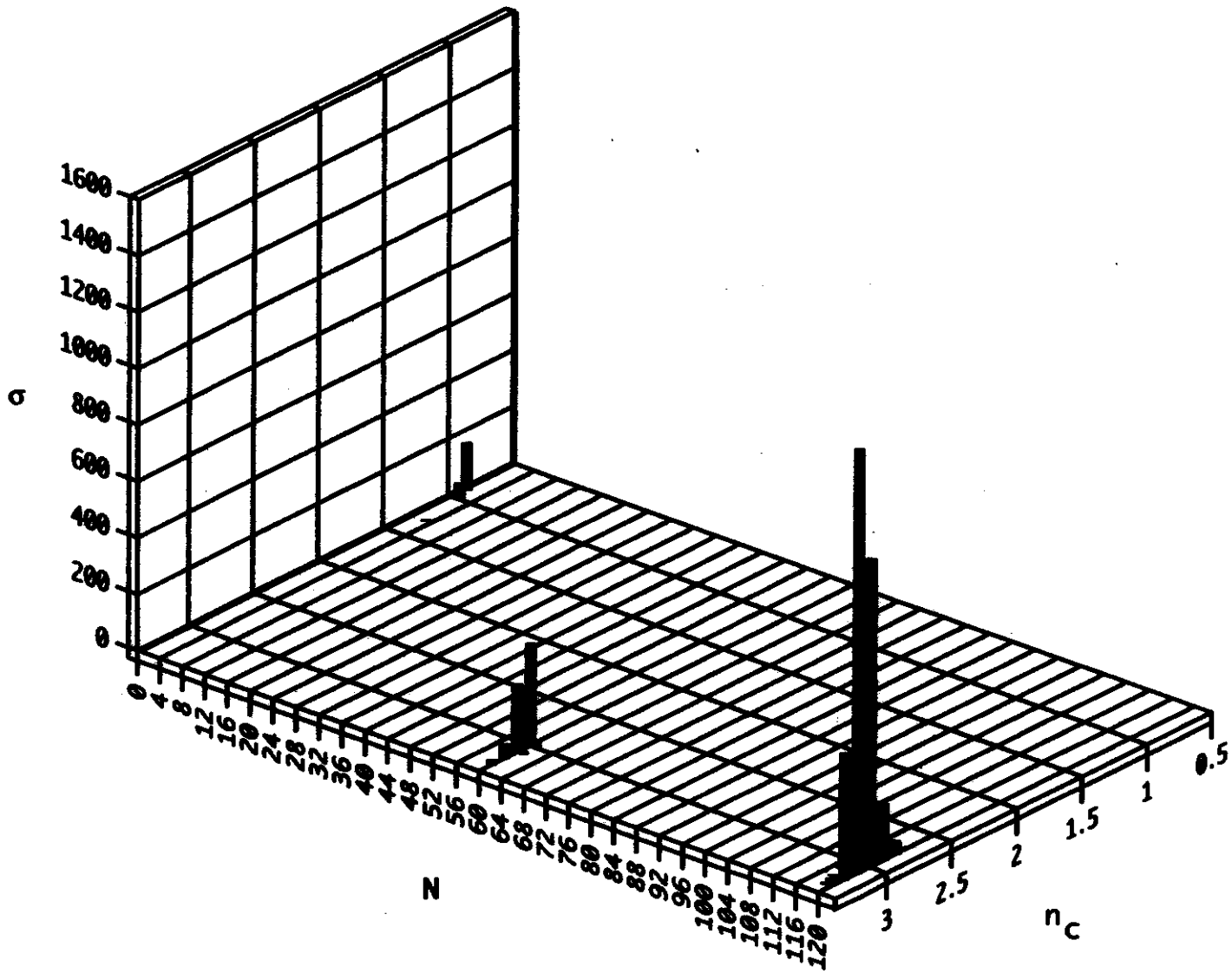

(0.039 ps)

J. Schulte, Phys. Rev. B, Fig. 1d

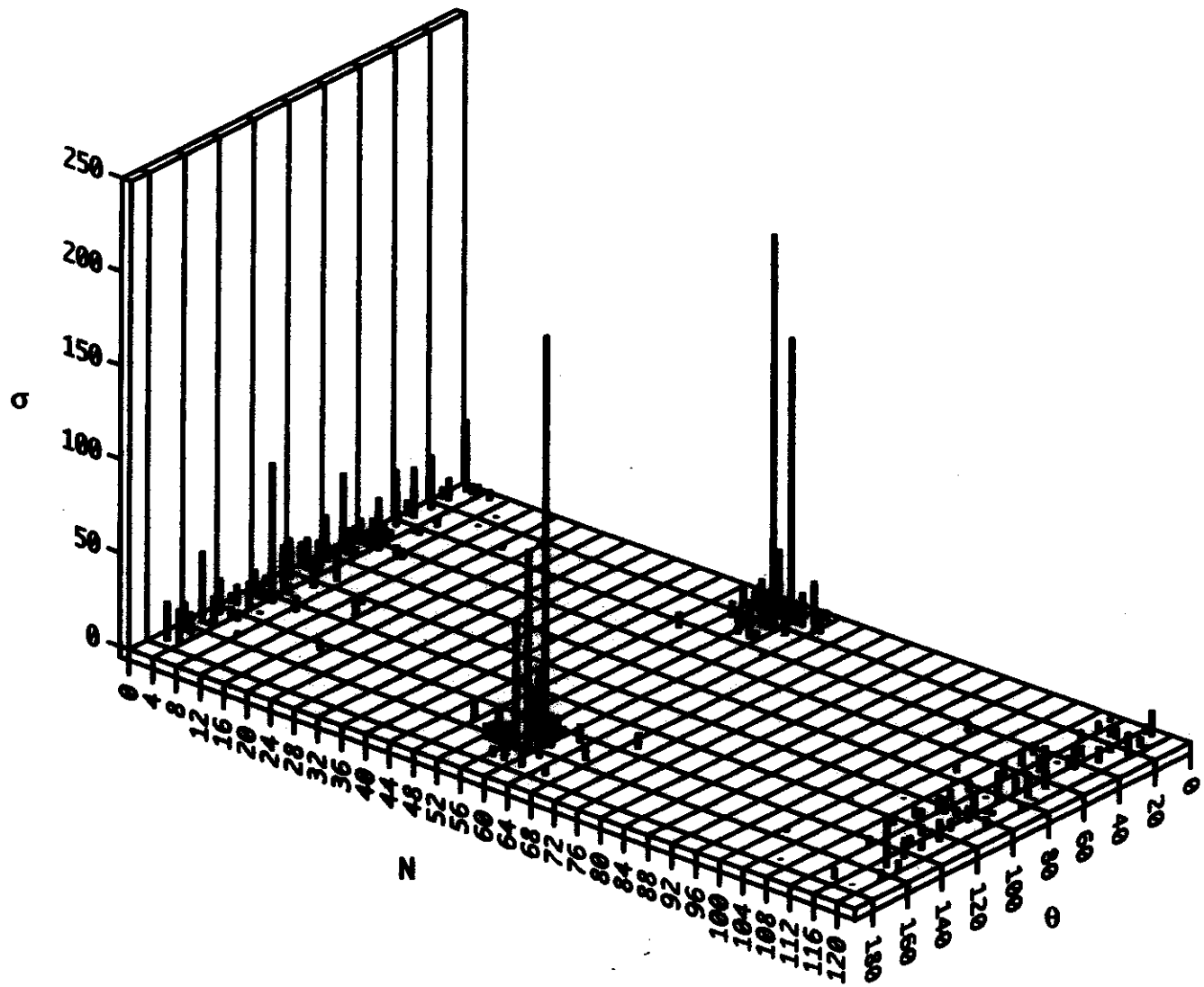

J. Schulte, Phys. Rev. B, Fig. 2a

(0.36 ps)

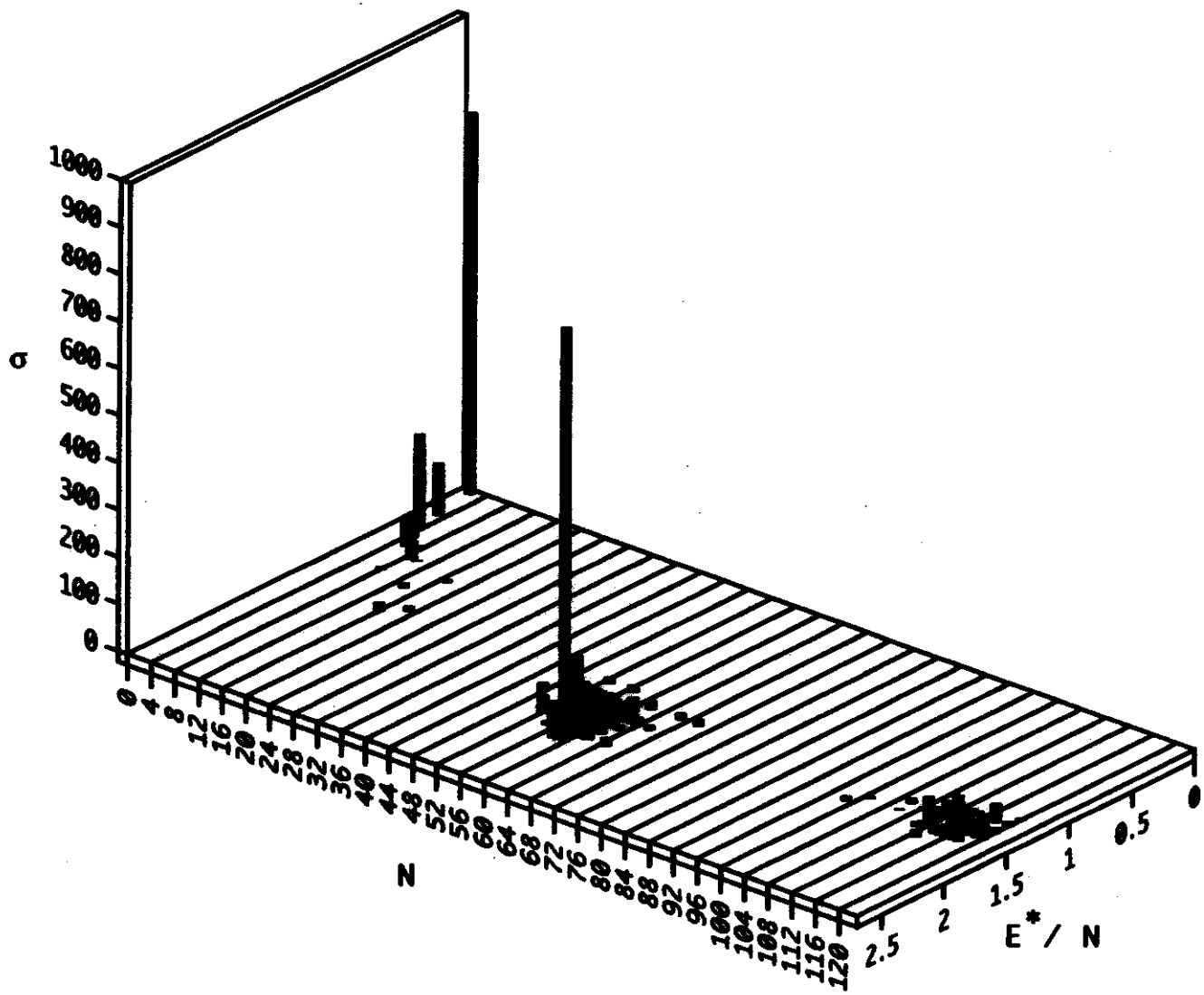

(0.36 ps)

J. Schulte, Phys. Rev. B, Fig. 2b

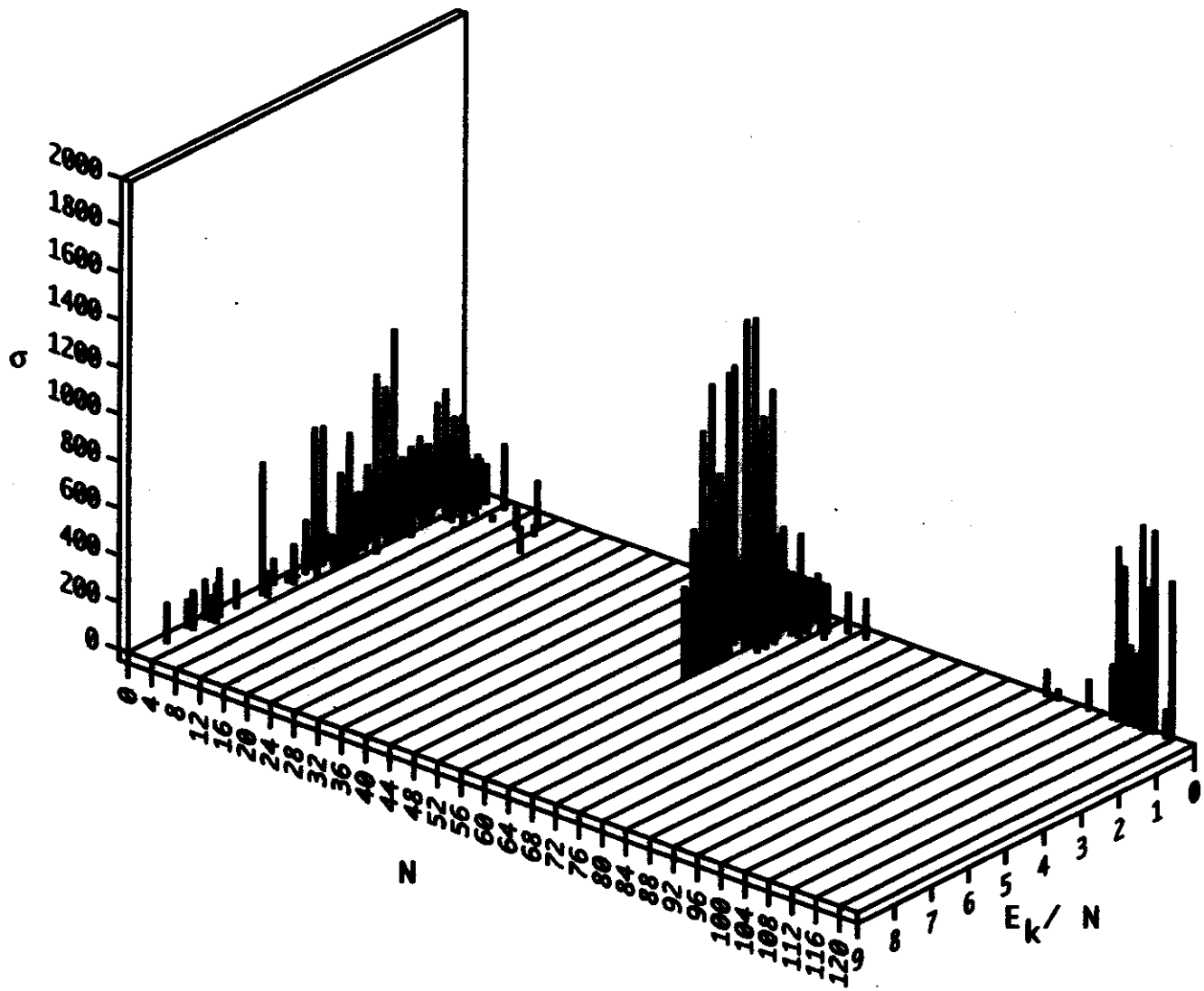

J. Schulte, Phys. Rev. B, Fig. 2c

(0.36 ps)

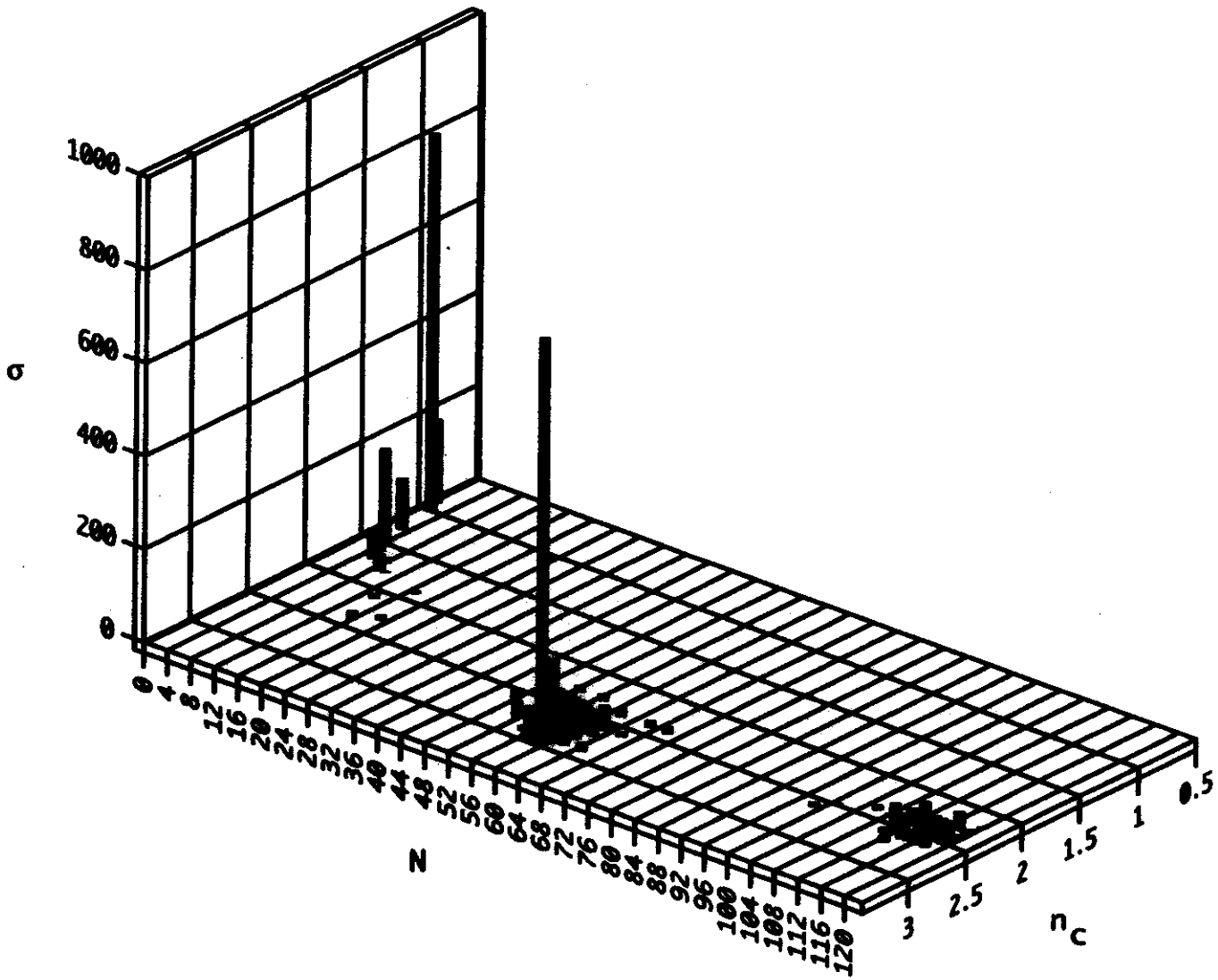

(0.36 ps) J. Schulte, Phys. Rev. B, Fig. 2d

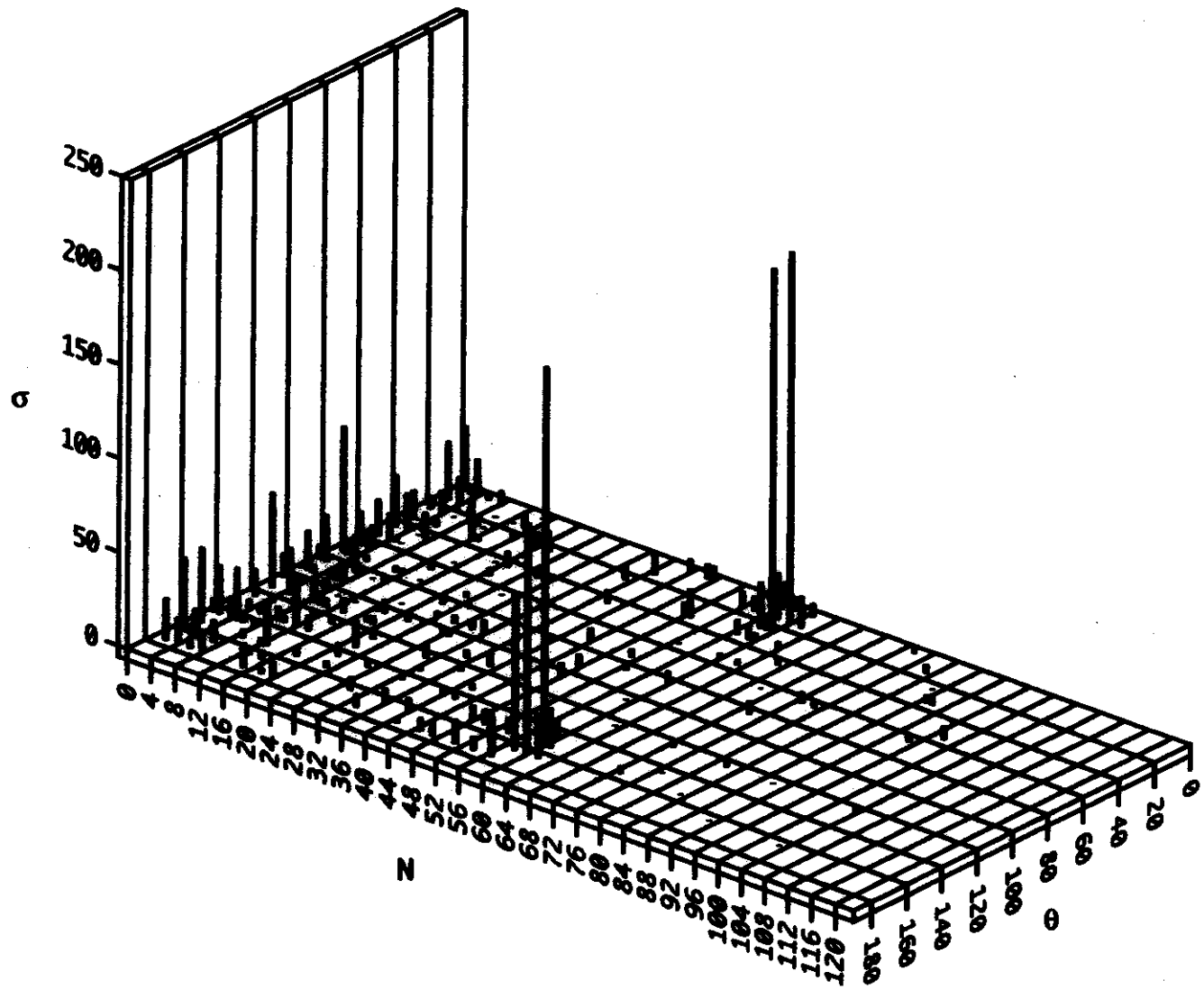

J. Schulte, Phys. Rev. B, Fig. 3a

(1.08 ps)

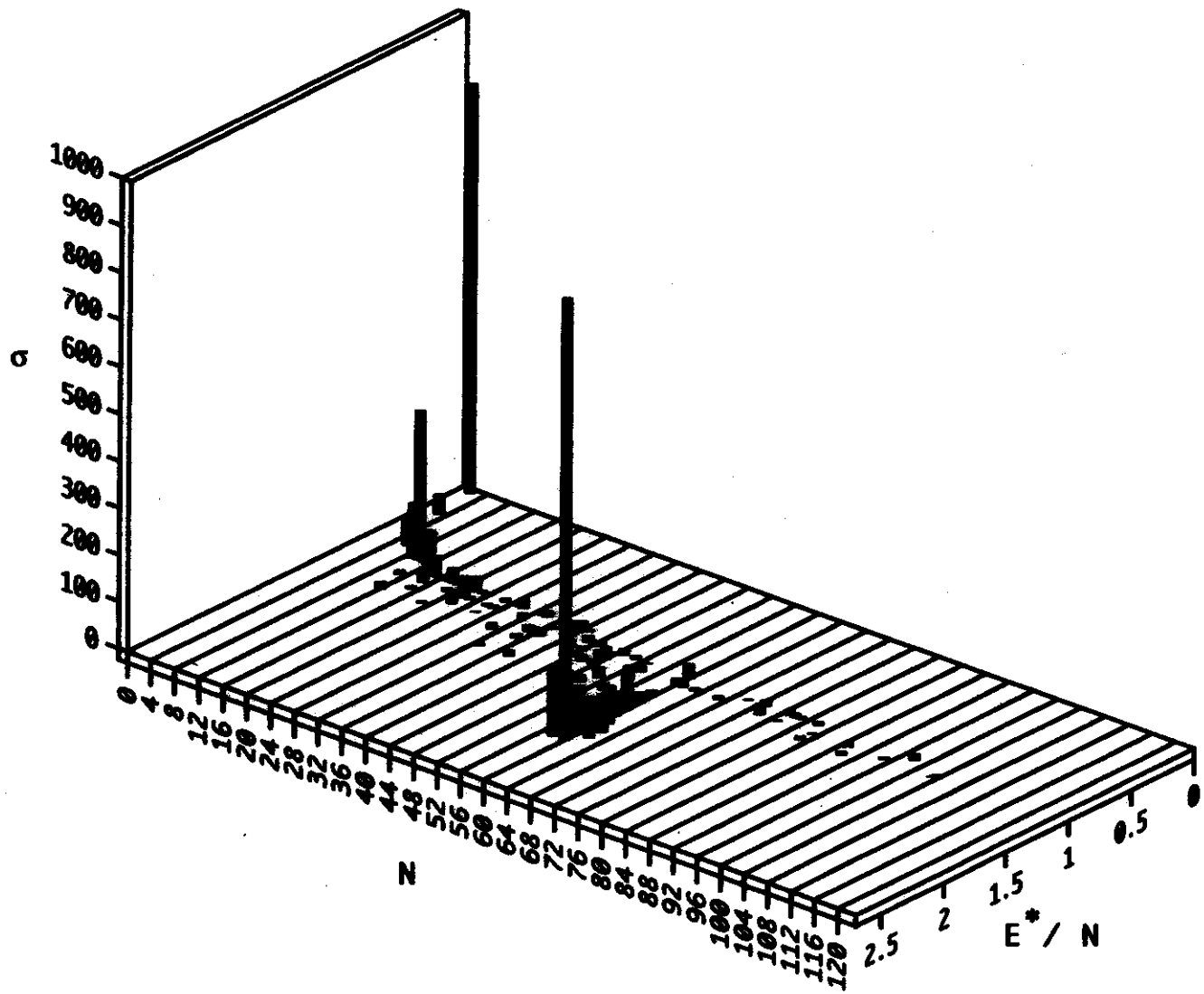

J. Schulte, Phys. Rev. B, Fig. 3b

(1.08 ps)

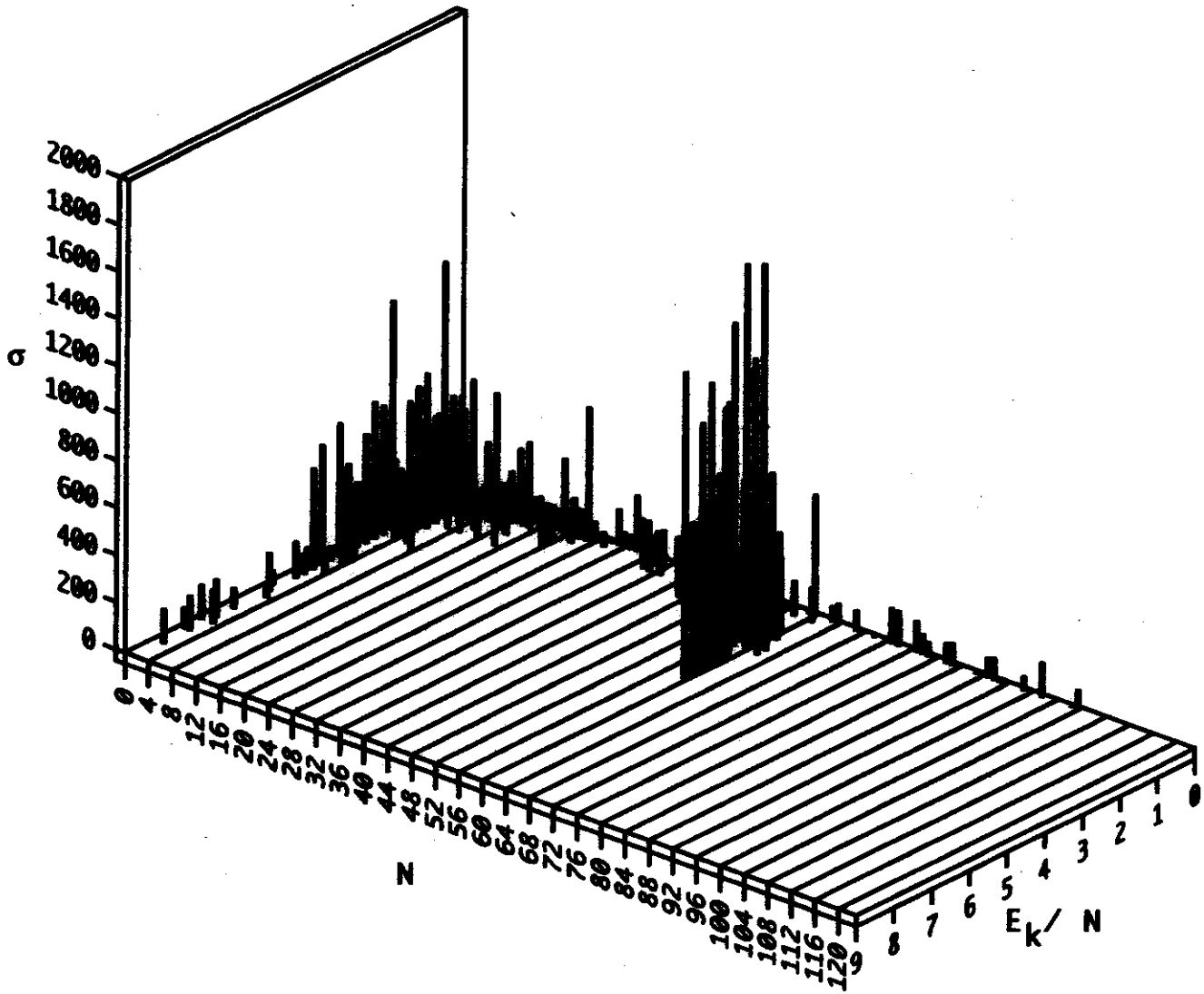

J. Schulte, Phys. Rev. B, Fig. 3c

(1.08 ps)

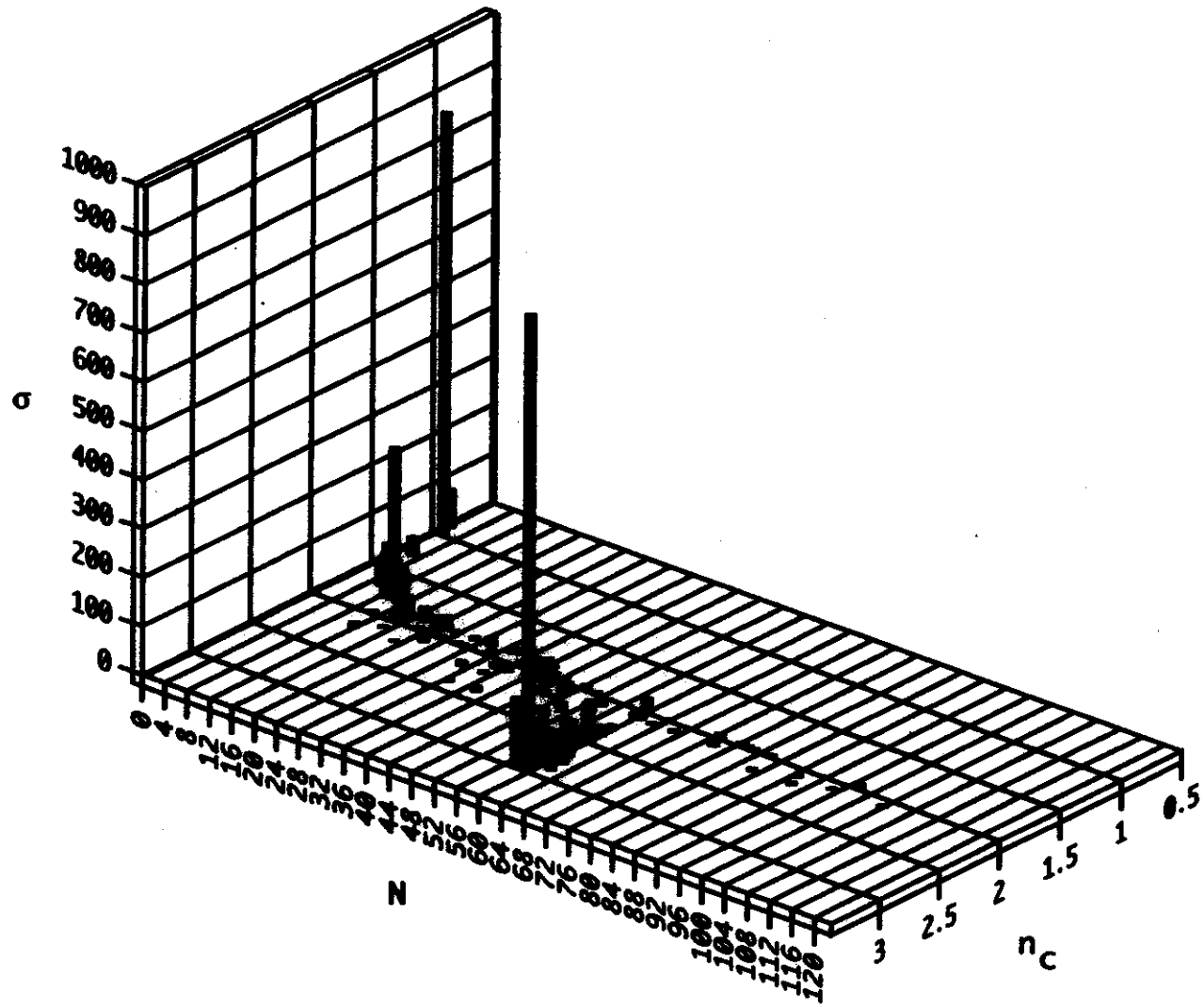

(1.08 ps)

J. Schulte, Phys. Rev. B, Fig. 3d

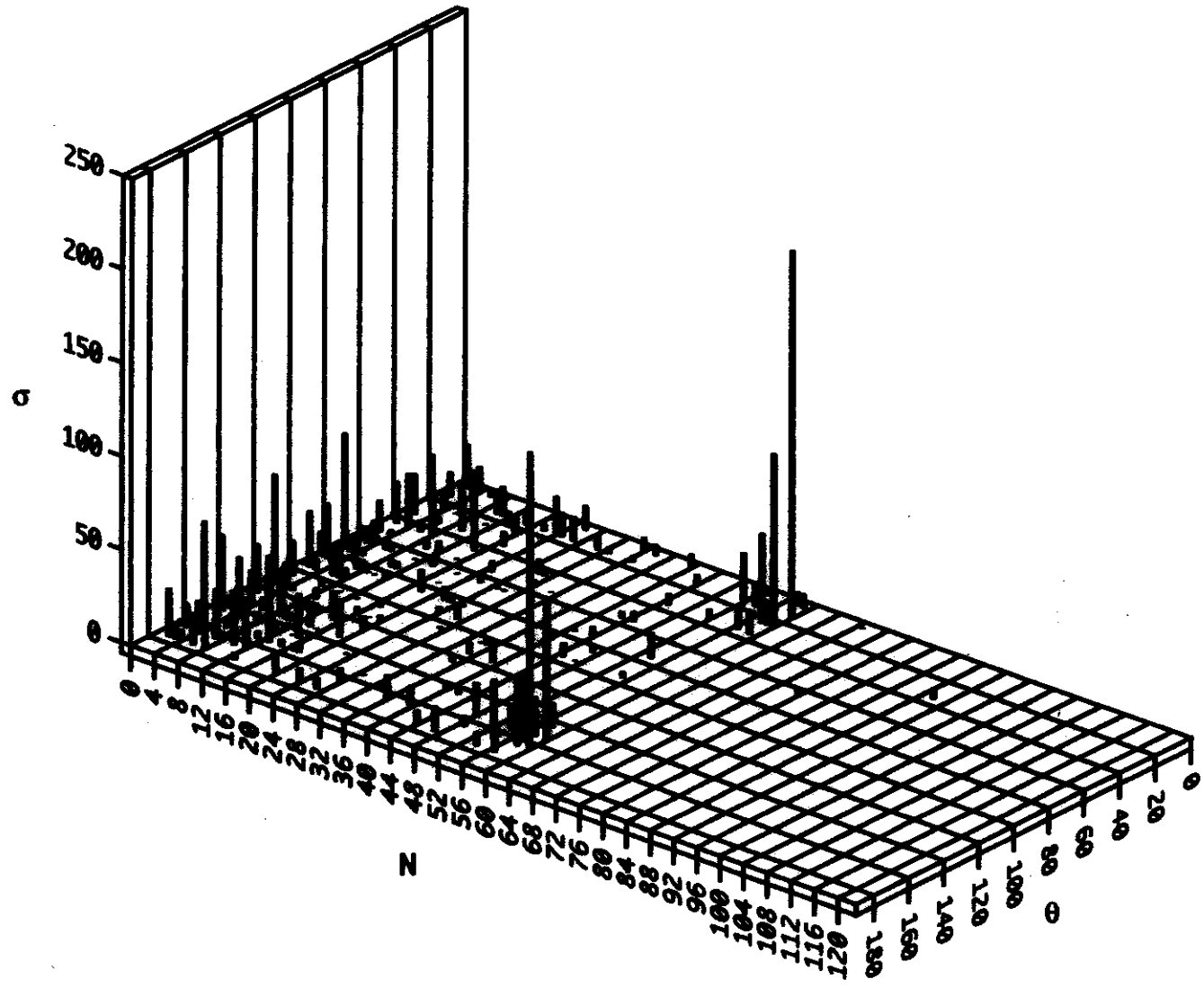

J. Schulte, Phys. Rev. B, Fig. 4a

(2.1 ps)

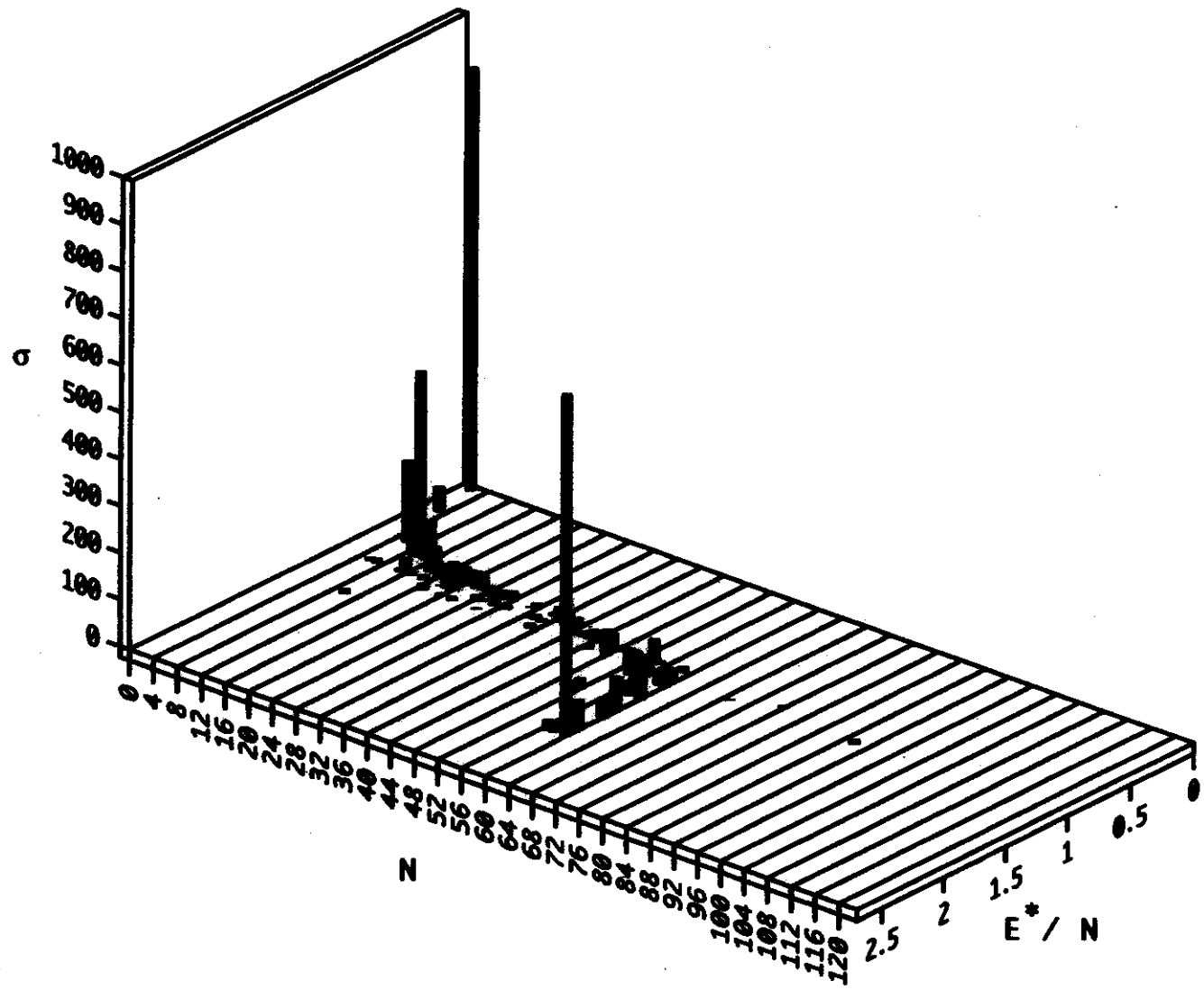

J. Schulte, Phys. Rev. B, Fig. 4b

(2.1 ps)

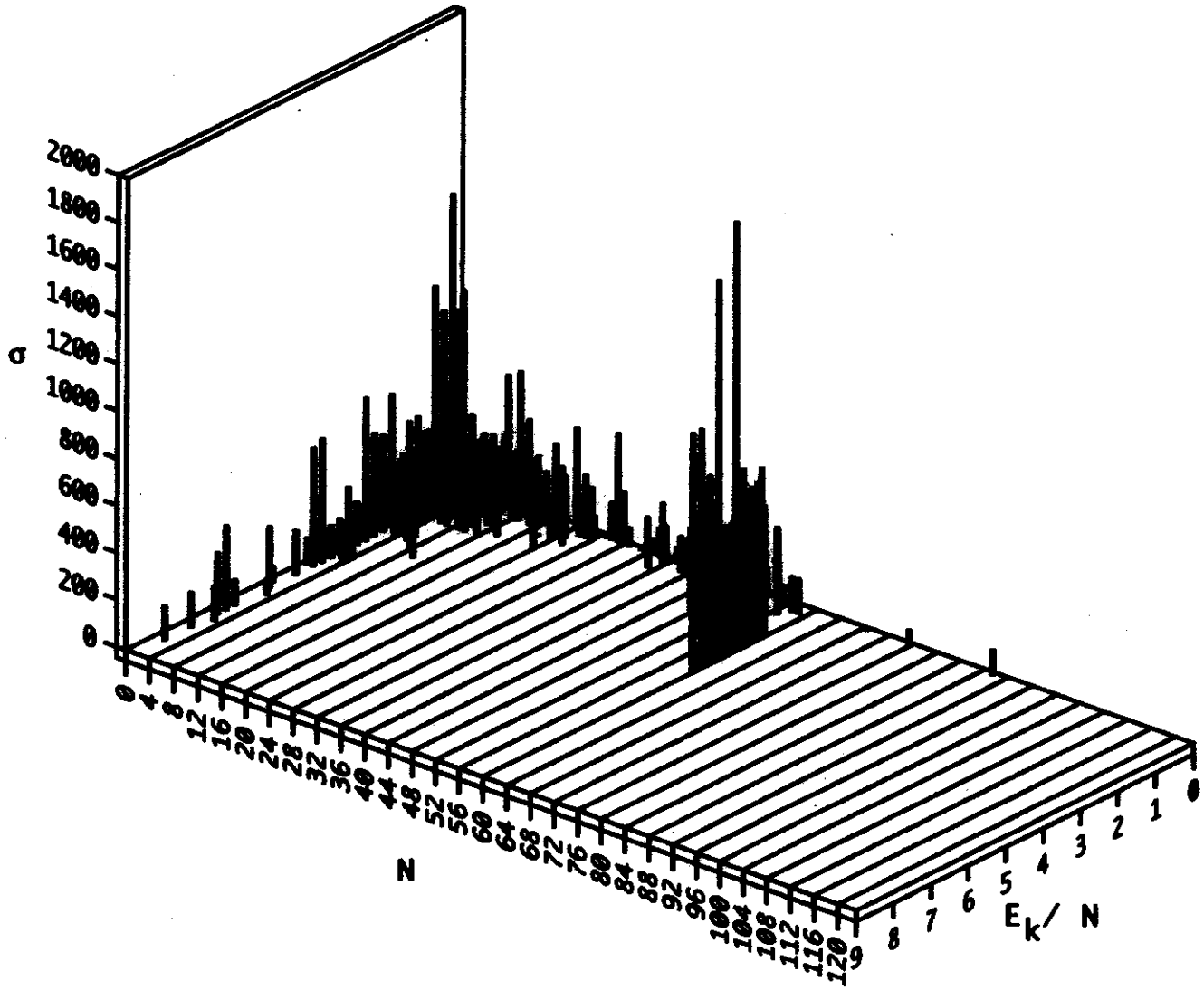

J. Schulte, Phys. Rev. B, Fig. 4c

(2.1 ps)

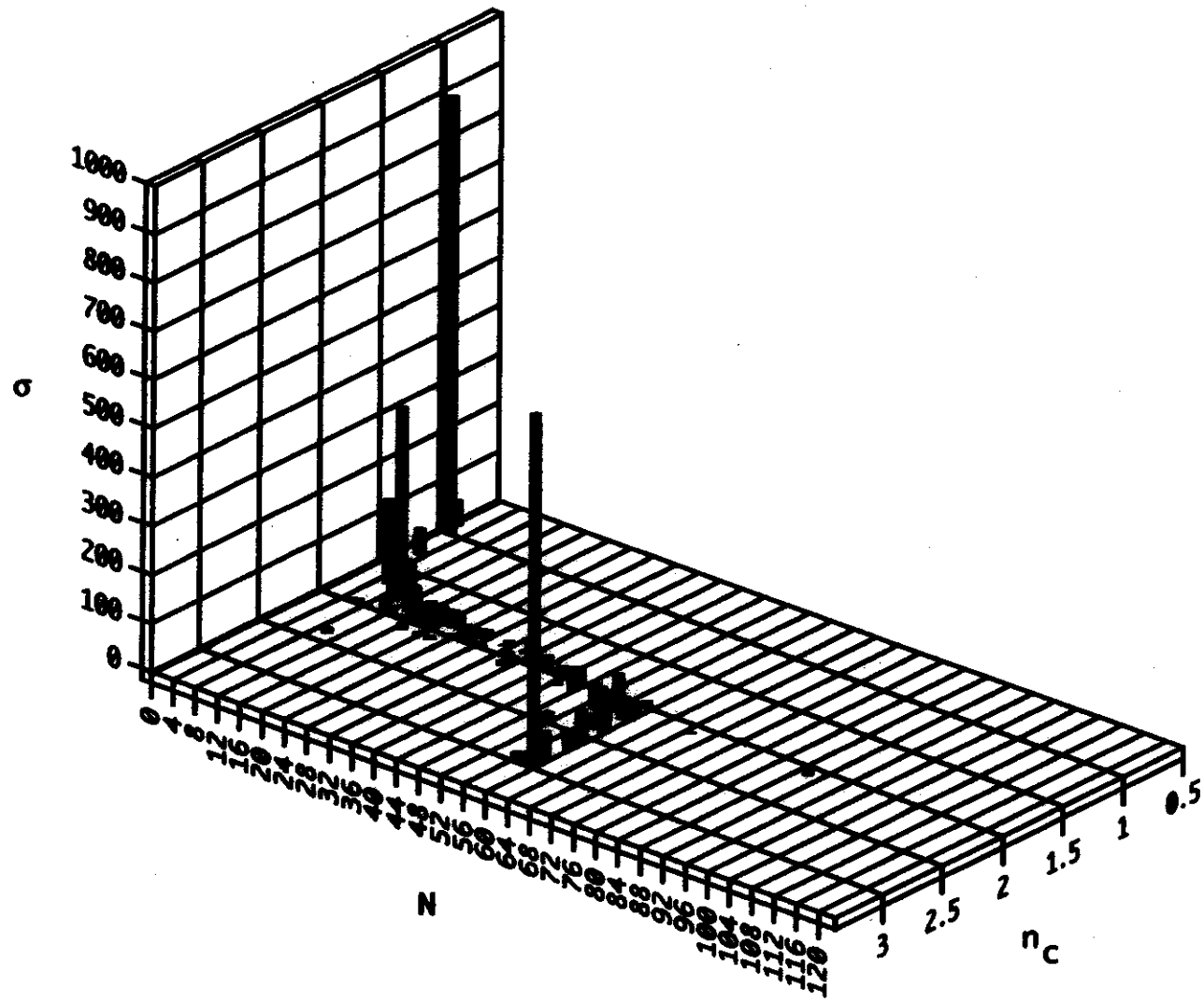

(2.1 ps)

J. Schulte, Phys. Rev. B, Fig. 4d

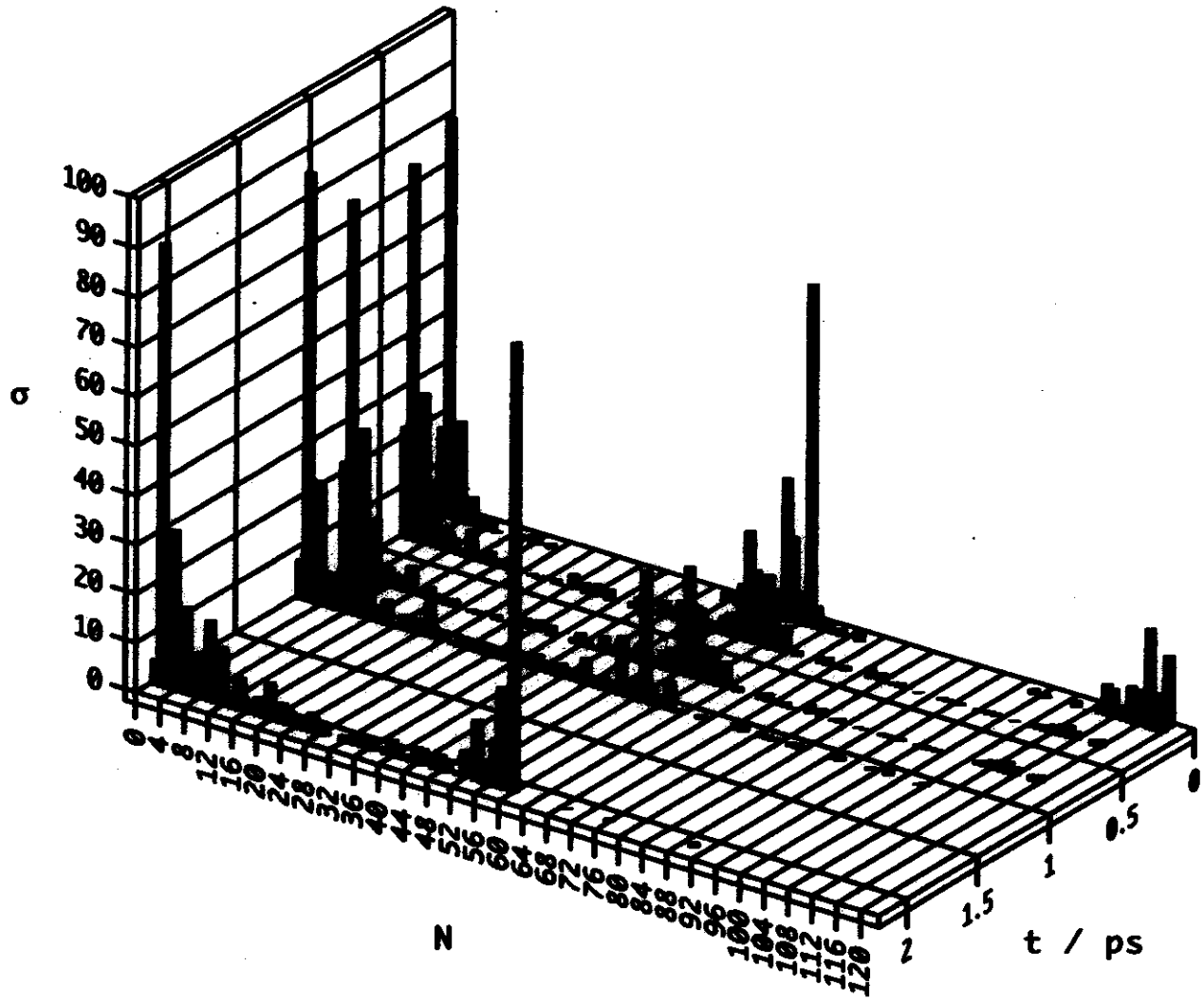

J. Schulte, Phys. Rev. B, Fig. 5

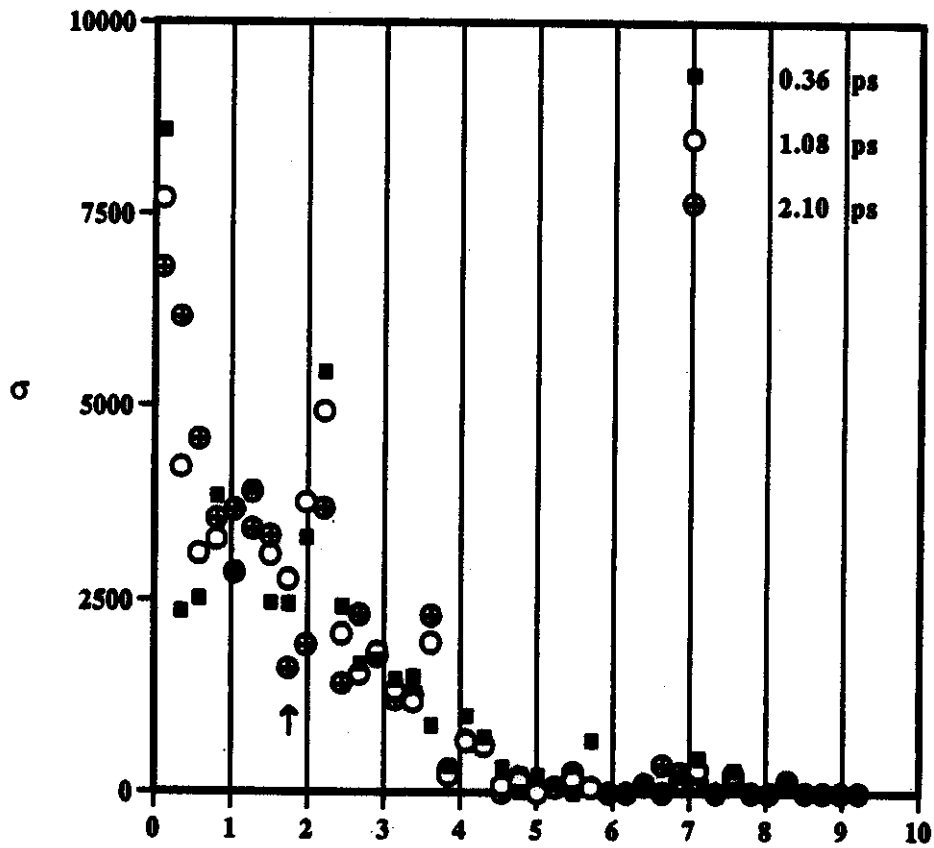

J. Schulte, Phys. Rev. B, Fig. 6a